Broadband X waves with orbital angular momentum

Miguel A. Porras and Raúl García-Álvarez
Grupo de Sistemas Complejos, ETSIME, Universidad Politécnica de Madrid, Rios Rosas 21, 28003 Madrid, Spain

(Received 10 October 2021; accepted 21 December 2021; published 6 January 2022)

We describe a class of minimal diffraction-free and dispersion-free superluminal wave packets (X waves and focused X waves) that can carry a given amount of units m of orbital angular momentum (OAM) per photon. Even if their frequency spectrum is wide enough to synthesize a unipolar pulse, OAM imposes a temporal pulse shape with as many zeros as units of OAM, and therefore $|m|/2$ temporal oscillations. All the frequencies in the broadband spectrum are displayed, like in a rainbow, from the bluer ones in the vicinity of the vortex to the redder ones in the wave periphery. At the same time, the whole wave packet experiences a blueshift proportional to $|m|$. As a result of the radial redshift and the OAM blueshift, the color of the brilliant ring around the central vortex is independent of OAM, and solely determined by the broadband source spectrum. Given the very peculiar properties of X waves with OAM, their generation and use, instead of standard Laguerre-Gauss modes, could improve the performance of OAM-based communication and quantum cryptographic systems, as well as the efficiency of the generation of high harmonics and attosecond pulses with OAM.

DOI: 10.1103/PhysRevA.105.013509

I. INTRODUCTION

X waves are diffraction-free and dispersion-free wave packets localized in space and time traveling at arbitrary superluminal group velocities in free space [1,2]. As particular members of the broader family of localized waves [2–5] (now renamed as space-time wave packets [6,7]), their spatiotemporal characteristics and experimental generation have deserved decades of research. Most of this research is focused on localized waves without orbital angular momentum (OAM) [2–5], and more recently on synthesizing one-dimensional localized waves, or space-time light sheets [6,7], which cannot carry OAM. This fact could seem surprising since the interest in OAM of light started and developed over the same decades, at first for monochromatic light [8,9], and later for ultrashort pulses [10–14]. Only recently vortex-carrying X waves and other diffraction-free pulses with OAM have started to gain attention [15–19].

Localized waves with cylindrical symmetry are built as coherent superpositions of diffraction-free Bessel beams of order $m = 0$ (without OAM) or $m \neq 0$ (with OAM) of different frequencies ω and weights $f(\omega)$. The integer m is the topological charge of the vortex in their center. Localized waves are dispersion free because the ω-dependent cone angle of the Bessel beams, $\theta(\omega)$, is such that the axial wave number (projection of the wave vector onto the propagation direction, say z) follows the linear variation law with frequency $k_z(\omega) = (\omega/c)\cos\theta(\omega) = a + \omega/v_g$, where a is an arbitrary constant and v_g is the group velocity. X waves are characterized by $v_g > c$ and $a = 0$, and focused X waves [20] are characterized by $v_g > c$ and $a \neq 0$.

The recent theoretical studies in Refs. [15–17] on X waves with OAM have unveiled a rather complex OAM-temporal coupled structure obeying certain universal constraints. In Refs. [15,16] the OAM-temporal couplings in the immediate vicinity of the vortex singularity are examined. With the same spectrum $f(\omega)$, the number of oscillations and their frequency increase with the magnitude of the topological charge, $|m|$. On the other hand, the bright ring surrounding the vortex is studied in Ref. [17]. In X waves built with the same $f(\omega)$, X waves have increasing duration at this ring when $|m|$ is increased, while the local frequency of the oscillations does not experience appreciable change with $|m|$, but is solely determined by the particular spectrum $f(\omega)$ of Bessel beams, e.g., the central frequency ω_f for bell-shaped spectra. The dependence of the duration of X waves on m originates from the lower bound $\Delta t \gtrsim |m|/\omega_f$ satisfied by all X waves at their bright ring.

Thus, to date, there is no a complete picture of the spatiotemporal structure of OAM-carrying X waves except in the vicinity of the vortex and the bright ring. Here we describe the spatiotemporal structure of X waves and focused X waves with OAM and with the broadband spectrum $f(\omega) = e^{-\epsilon\omega}$, where ϵ is a small quantity for $f(\omega)$ to cover from a dc component to the optical spectrum and beyond, as in Fig. 1(a). Without OAM, the fundamental X wave is nonoscillatory in time, and therefore is of little interest in optics; indeed only X waves with narrower spectra about microwave [21] and optical frequencies [2], called Bessel-X waves, [22] have been generated. However, the introduction of OAM eliminates any component about $\omega = 0$ and induces what can be qualified as intrinsic temporal oscillations associated with OAM, the frequency of which can be tuned in any range of the electromagnetic spectrum. The previously described OAM-temporal couplings [15–17] arise here naturally as a result of the whole spatiotemporal coupled structure of these X waves with OAM.

The OAM-induced oscillations feature a number of zeros approximately equal to $|m|$, and hence $|m|/2$ oscillations.

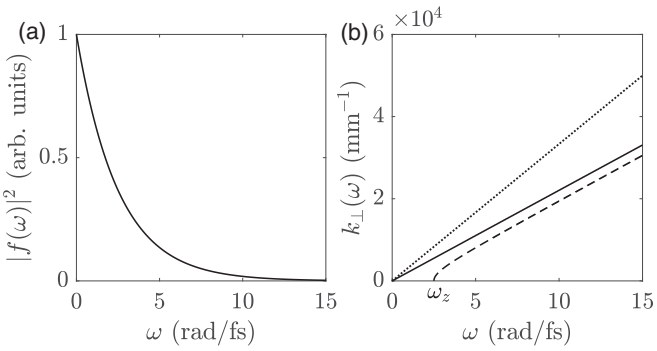

FIG. 1. (a) Spectral density of the broadband Bessel beam spectrum $f(\omega) = \exp(-\epsilon\omega)$ with $\epsilon = 0.2$ fs, spanning the visible spectrum and beyond. (b) Transversal wave numbers of the X wave with $v_g = 0.0004$ mm/fs (solid line), of the focused X wave with the same velocity and $\omega_z = 2.5$ rad/fs ($a = 2.083 \times 10^3$ mm^{-1}) (dashed curve), and ω/c (dotted line).

Since the same number of oscillations fill the inside of the X arms at any radial distance from the vortex singularity, their frequency is redshifted radially outwards down to zero at infinity (with zero amplitude). With increasing $|m|$, the entire X wave is blueshifted, at the same time that the bright ring is displaced outwards, resulting in a frequency at this ring independent of the topological charge. The structure of focused X waves closely resembles that of X waves in their inner part, but the number of oscillations becomes increasingly larger than those of X waves of the same OAM towards the periphery. In addition, the oscillations spread temporally out of the X arms in the outer radial part, and their frequency approaches a nonzero constant value.

The duration of the broadband X waves at their bright ring is found to coincide with the lower bound $|m|/\omega_f$ described in Ref. [17]. Therefore broadband X waves are minimal X waves capable to carry a given amount of OAM. Being diffraction free, dispersion free, and minimal OAM carriers (and having other properties such as self-healing behavior and turbulence resistance [23]), broadband X waves appear as optimum wave modes in many applications, particularly in superdense, multichannel free-space communications [24], and free-space quantum communications systems [25,26], commonly based on Laguerre-Gauss-type modes.

II. SUPERLUMINAL LOCALIZED WAVES WITH OAM

A quite general expression of cylindrically symmetric localized waves with OAM is $E(r, \varphi, t, z) = E(r, t, z)e^{im\varphi}$, with

$$E(r, z, t) = \frac{e^{iaz}}{\pi} \int_{0,\, k_\perp \text{real}}^{\infty} d\omega f(\omega) J_m[k_\perp(\omega) r] e^{-i\omega t'}, \qquad (1)$$

where (r, φ, z) are cylindrical coordinates, $t' = t - z/v_g$ is the local time for the group velocity v_g, and $k_\perp(\omega) = (\omega/c)\sin\theta(\omega) = \sqrt{(\omega/c)^2 - k_z^2(\omega)}$ is the transversal wave number (modulus of the transversal projection of the wave vector), or, given the linear variation of $k_z(\omega)$,

$$k_\perp(\omega) = \sqrt{\left(\frac{\omega}{c}\right)^2 - \left(a + \frac{\omega}{v_g}\right)^2}. \qquad (2)$$

The integral has been limited to nonnegative positive frequencies to yield the analytical signal complex representation of the electric field, the real part of which is the real field. The limitation to real $k_\perp(\omega)$ expresses the restriction that the axial wave number $a + \omega/v_g$ cannot be higher than ω/c. The electric field of X waves ($a = 0$, $v_g > c$) does not depend on z. The transversal wave number is the straight line $k_\perp(\omega) = (\sin\theta/c)\omega$ crossing the origin $\omega = 0$ of slope $\sin\theta/c$ [Fig. 1(b)], corresponding to a constant cone angle $\theta = \sin^{-1}(c\sqrt{1/c^2 - 1/v_g^2})$. For focused X waves ($a \neq 0$, $v_g > c$) the electric field oscillates with axial period $2\pi/a$. The transversal wave number $k_\perp(\omega)$ is a branch of hyperbola starting at some positive frequency ω_z (the other branch is entirely in $\omega < 0$), the same asymptotic slope $\sin\theta/c$ as the X wave of the same v_g [Fig. 1(b)], and a ω-dependent cone angle approaching θ at large ω. We will fix the frequency ω_z as an important frequency of focused X waves by setting

$$a = \omega_z\left(\frac{1}{c} - \frac{1}{v_g}\right), \qquad (3)$$

so that $\omega_z = 0$ specifies an X wave, and $\omega_z > 0$ specifies a focused X wave [see Fig. 1(b)].

A. Broadband X waves with OAM

Taking, as in Ref. [1], the broadband exponential spectrum $f(\omega) = \exp(-\epsilon\omega)$, and setting $a = 0$ ($\omega_z = 0$) and $k_\perp(\omega) = (\sin\theta/c)\omega$, the integral in (1) can be carried out to yield

$$E(r, z, t) = \frac{1}{\pi\sqrt{(\epsilon + it')^2 + \left(\frac{\sin\theta}{c} r\right)^2}} \times \frac{\left(\frac{\sin\theta}{c} r\right)^{|m|}}{\left[\sqrt{(\epsilon + it')^2 + \left(\frac{\sin\theta}{c} r\right)^2} + \epsilon + it'\right]^{|m|}} \qquad (4)$$

[and multiplied by $(-1)^{|m|}$ if $m < 0$]. Equation (4) was already derived in the pioneering work of Lu and Greenleaf [1]: The integrals involved in obtaining the expression for the fundamental, OAM-free X wave were performed with Bessel functions of arbitrary order m. The expression with $m \neq 0$, however, received no attention either in that work or subsequently, to the best of our knowledge.

The electric field approaches zero as $r^{|m|}$ close to the vortex singularity, and as $1/r$ at large enough distances, carrying then infinite energy, as the OAM-free X wave. In Figs. 2(a)–2(d) the real electric field of X waves without and with OAM can be compared. There is no light at times immediately outside the X arms, so that the duration at each radial distance is the time between the X arms, $2\Delta t = 2(\sin\theta/c)r$.

The most evident and relevant difference is that with $m = 0$ the electric field is a unipolar pulse that splits into two unipolar pulses, while with $m \neq 0$ the temporal pulse shape at any radial distance has approximately $|m|$ zeros, or more precisely, the smallest even number greater than or equal to $|m|$, e.g., 2 for $|m| = 1, 2$; 4 for $|m| = 3, 4$; and so on. The number of

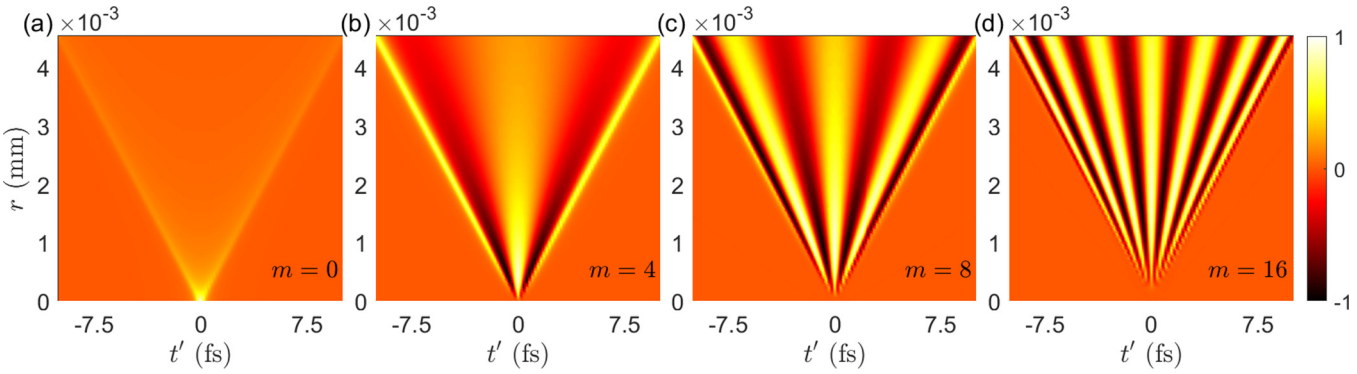

FIG. 2. Real electric field of X waves with $v_g = 0.0004$ mm/fs, $\epsilon = 0.2$ fs and the indicated topological charges. All fields are normalized to their respective peak values.

oscillations may slightly differ depending on the particular criterion. According to the instantaneous frequency analysis below, the number of oscillations is $|m|/2$ irrespective of whether m is even or odd. These oscillations are more clearly seen in Figs. 3(a)–3(c) for $|m| = 8$ at different radial distances. Thus, the increase of the number of oscillations with the magnitude of the topological charge does not only pertain to the vicinity of the vortex, as reported in Ref. [15], but to the whole X wave. These are intrinsic oscillations associated with OAM, and result from the fact that the inverse Fourier transform $\int_0^\infty J_m[(\sin\theta/c)\omega r]e^{-i\omega t}d\omega$ has these zeros and oscillations. The exponential $e^{-\epsilon\omega}$ does not remove them, but only makes those at the trailing and leading parts of the pulse have smaller and smaller amplitude towards the vortex center, as seen in the temporal shapes in Figs. 3(a)–3(c). This softening is the result of the increasing apodization of the Bessel function by the exponential spectrum towards the vortex center, as observed in the respective spectral densities in Figs. 3(d)–3(f).

With a fixed number of oscillations at all radii within a linearly increasing time interval $2\Delta t = 2(\sin\theta/c)r$ between the X arms, their frequency must decrease approximately inversely proportional to r. Also, with a number of oscillations proportional to $|m|$, their frequency at any particular radius r must increase proportionally to $|m|$.

For a more quantitative analysis, we consider the instantaneous frequency, defined as $\omega_c = -d\arg E/dt'$, which can also be evaluated from

$$\omega_c(r,t') = -\mathrm{Re}\left\{\frac{\int_0^\infty e^{-\omega(\epsilon+it')}J_m[k_\perp(\omega)r]\omega d\omega}{\int_0^\infty e^{-\omega(\epsilon+it')}J_m[k_\perp(\omega)r]d\omega}\right\}, \quad (5)$$

yielding

$$\omega_i(r,t') = \mathrm{Re}\left\{\frac{|m|\sqrt{(\epsilon+it')^2+\left(\frac{\sin\theta}{c}r\right)^2}+(\epsilon+it')}{(\epsilon+it')^2+\left(\frac{\sin\theta}{c}r\right)^2}\right\}. \quad (6)$$

Simple inspection shows that $\omega_i(r,t')$ takes a minimum value

$$\omega_c(r) \equiv \omega_i(r,t'=0) = \frac{|m|\sqrt{\epsilon^2+\left(\frac{\sin\theta}{c}r\right)^2}+\epsilon}{\epsilon^2+\left(\frac{\sin\theta}{c}r\right)^2}, \quad (7)$$

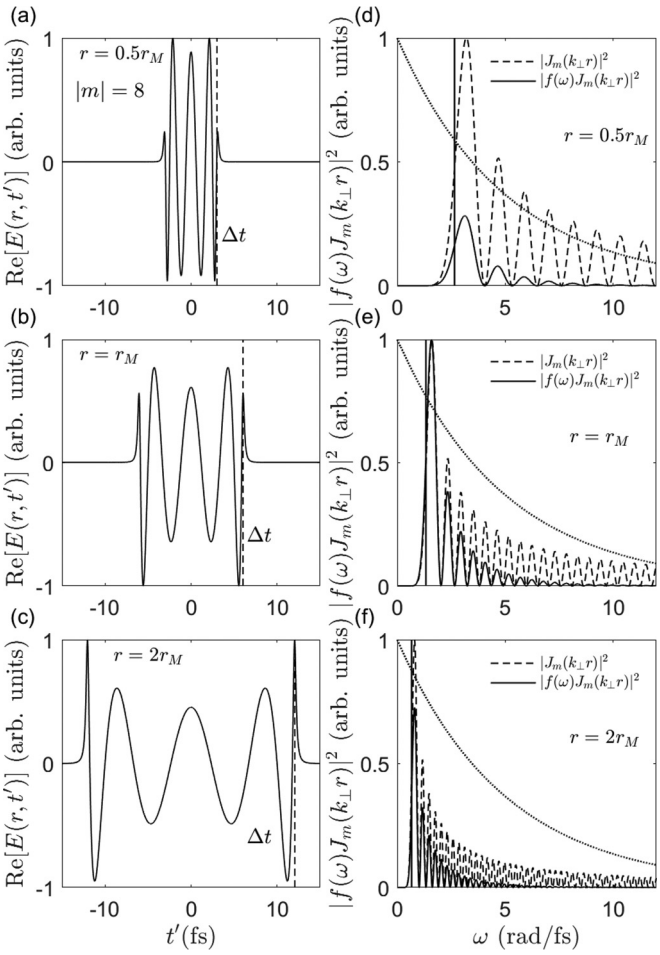

FIG. 3. [(a)–(c)] Real electric field of X waves with $v_g = 0.0004$ mm/fs, $\epsilon = 0.2$ fs, and $|m| = 8$ at (a) $r = 0.5r_M$, (b) $r = r_M$, and (c) $r = 2r_M$, where r_M is the radial distance of maximum fluence. $\Delta t = (\sin\theta/c)r$ indicates the location of the X arms, where the X wave terminates. All fields are normalized to their peak values. (d–f) Respective power spectra (solid curves), the Bessel factor $J_m(k_\perp r)$ (dashed curves), and the broadband spectrum factor $f(\omega) = e^{-\epsilon\omega}$ (dotted curves). The vertical lines indicate the central frequency about $t' = 0$, $\omega_c(r)$, coinciding with the first rise of the Bessel functions in each case.

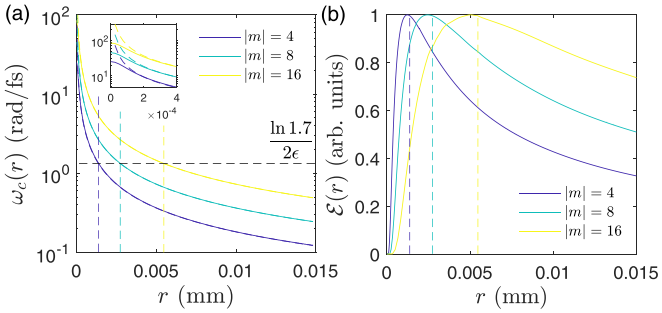

FIG. 4. (a) Central instantaneous frequency of the oscillations, $\omega_c(r)$, as a function of the radius r for the indicated values of $|m|$ of X waves with $v_g = 0.0004$ mm/fs and $\epsilon = 0.2$ fs, as given by the exact expression (7) (solid curves) and the approximate expression (8) (dashed curves). They are almost indistinguishable except in the immediate vicinity of the vortex singularity. This region is enlarged in the inset. (b) Radial profiles of fluence of the same X waves, numerically evaluated from (12), and normalized to their peak values. In (a) and (b) the vertical lines are r_M given by (13), locating approximately the radii of maximum fluence. The horizontal line in (a) helps to visualize that the central instantaneous frequency $\omega_f = \ln(1.7)/2\epsilon$ is the same at the respective radii of maximum fluence, i.e., independent of m. Violet (dark gray), green (gray), and yellow (light gray) curves are for $|m| = 4, 8, 16$, respectively.

at $t' = 0$, or central instantaneous frequency, that remains almost constant in time except in the vicinity of the X arms, and is plotted as a function of r for several values of $|m|$ in Fig. 4(a). As the minimum frequency at each radial distance, it coincides with the first rise of the Bessel function in the spectrum, indicated by vertical lines in Figs. 3(d)–3(f). In fact a good approximation to (7) can be derived by equating the argument $x = k_\perp r = (\sin\theta/c)\omega r$ of the Bessel function $J_m(x)$ to that of the first rise of the Bessel function, $x \simeq |m|$, which yields

$$\omega_c(r) \simeq \frac{|m|}{(\sin\theta/c)r}. \tag{8}$$

This approximate equality is seen in Fig. 4(a) to fit accurately (7) except in a tiny radial region [see inset in Fig. 4(a)] about the vortex (compared to the radius of maximum X-wave energy, r_M). Thus, except in that region, the frequency $\omega_c(r)$ is independent of the particular broadband spectrum defined by ϵ, and is inversely proportional to r, as expected. For $r \to 0$, the exact formula (7) yields the finite value

$$\omega_c(0) = \frac{|m|+1}{\epsilon}, \tag{9}$$

which is similar to the result in Refs. [15,16]. From the latter relation and (8), we also conclude that the blueshift proportional to the magnitude of the topological charge not only takes place in the vicinity of the vortex, but affects the whole X wave.

Equation (6) for the instantaneous frequency at any time allows us to evaluate the number of oscillations within the X arms. In the same way as $\omega_c(r)$, $\omega_i(r,t')$ in (6) turns out to be almost independent of ϵ, except in the vicinity of the X arms, and to be approximately given by

$$\omega_i(r,t') \simeq \frac{|m|}{\sqrt{\left(\frac{\sin\theta}{c}r\right)^2 - t'^2}} \tag{10}$$

provided that $|t'| < \Delta t = (\sin\theta/c)r$, i.e., within the X arms. Averaging in this time interval (integrating and dividing by $2\Delta t$) yields an average instantaneous frequency at each radius as

$$\bar{\omega}_i(r) = \frac{\pi}{2}\frac{|m|}{(\sin\theta/c)r}. \tag{11}$$

One can then evaluate the number of oscillations as the full duration $2\Delta t$ over the average period $2\pi/\bar{\omega}_i(r)$, resulting in a number of oscillations equal to $|m|/2$.

The global blueshift of X waves with $|m|$ might lead one to think that the whole X wave becomes bluer and bluer with increasing magnitude of the topological charge. However, this is only the case in the immediate vicinity of the vortex, as seen in (9). According to (8), valid out of this region, any given frequency is displaced radially outwards as $|m|$ is increased. As shown below, the radius of maximum energy density (fluence), or bright ring to a time-integrating detector, is also displaced with increasing $|m|$ in such a way that the frequency of the bright ring is independent of m, and in this sense it can be said that X waves are of the same color irrespective of their OAM.

The fluence is given by $\mathcal{E}(r) = \int_{-\infty}^{\infty}(\mathrm{Re}E)^2 dt' = \frac{1}{2}\int_{-\infty}^{\infty}|E|^2 dt'$, or, in terms of the spectral density, by

$$\mathcal{E}(r) = \frac{1}{\pi}\int_0^\infty e^{-2\epsilon\omega}|J_m[k_\perp(\omega)r]|^2 d\omega, \tag{12}$$

which is plotted in Fig. 4(b) for several values of $|m|$ for illustration. Although the above integral does not admit analytical integration, detailed numerical inspection shows that the area of the product of $e^{-2\epsilon\omega}$ and $|J_m(k_\perp r)|^2$ is maximum, and then the fluence, at the radius r_M where the frequency of the first rise of $|J_m(k_\perp r)|^2$ is $\omega_c(r_M)$, coincides with the frequency ω_f at which the broadband spectral density $e^{-2\epsilon\omega}$ has decayed by about $1/1.7 = 0.588$ of its value at $\omega = 0$, i.e., $\omega_f \simeq \ln(1.7)/2\epsilon$. With this relative position, the Bessel function is not too damped and not too oscillatory, as exemplified in Figs. 3(d)–3(f). The frequency at the bright ring, $\omega(r_M) \simeq \omega_f$, is then independent of m, as illustrated in Fig. 4(a). The fact that the frequency at the bright ring is solely determined by $f(\omega)$ was also reported in Ref. [12] for X waves with bell-shaped spectra, and for ultrashort Laguerre-Gauss pulses in Refs. [12–14]. From (8) equated to ω_f, we obtain the radius of the bright ring as

$$r_M \simeq \frac{|m|}{\omega_f(\sin\theta/c)}, \tag{13}$$

which is proportional to $|m|$, and provides a good approximation to the exact radius [see Fig. 4(b)].

Also in Ref. [12], the lower bound to the duration at the bright ring of X waves carrying m units of OAM is established as $\Delta t \gtrsim |m|/\omega_f$ (half duration). Broadband X waves have just the minimum duration $\Delta t = (\sin\theta/c)r_M = |m|/\omega_f$, and are therefore minimal X waves capable to carry m units of OAM.

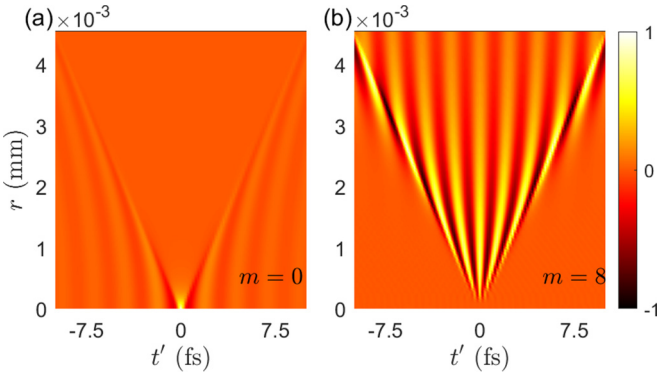

FIG. 5. Real electric field of focused X waves with $v_g = 0.0004$ mm/fs, $\omega_z = 2.5$ rad/fs, and $\epsilon = 0.2$ fs (a) without OAM and (b) with OAM.

B. Broadband focused X waves with OAM

Integral (1) with the exponentially decaying Bessel beam spectrum and $k_\perp(\omega)$ in (2) with $\omega_z \neq 0$ ($a \neq 0$) cannot generally be performed by analytical means. Only for $m = 0, 1$ the integral is written analytically in Ref. [27], but the expression is quite involved. As done for X waves, the relevant aspects of the spatiotemporal structure of focused X waves can more easily be extracted from an analysis of the spectrum, and from the resemblance to the X wave with $a = 0$ of the same group velocity and vorticity.

Without OAM, focused X waves and X waves differ substantially [compare Figs. 2(a) and 5(a)] because the spectrum $f(\omega)J_m(k_\perp r)$ of focused X waves with $m = 0$ is highly peaked at the positive cutoff frequency ω_z (where $k_\perp r = 0$) responsible for the infinite temporal oscillations observed at any radial distance. For focused X waves with OAM, however, the spectrum $f(\omega)J_m(k_\perp r)$ vanishes at ω_z, which removes these oscillations, and makes the focused X wave with OAM resemble much more the X wave with OAM [compare Figs. 2(c) and 5(b)].

In the vicinity of the vortex the number of oscillations is indeed the same as that of the X wave of the same vorticity [Fig. 6(a)]. This feature can be understood from the fact that the slope of $k_\perp(\omega)$ at high frequencies is the same as for the X wave [Fig. 1(b)], and that these high frequencies are located in the vicinity of the vortex. The cutoff frequency ω_z plays a negligible role in the spectrum at these distances [Fig. 6(d)]. Moving towards the periphery the number of oscillations becomes gradually larger than that of the X wave, growing without bound and approaching the constant frequency ω_z [Fig. 6(b)] because the spectrum approaches ω_z [Fig. 6(e)] with increasing radius. At large enough radius [Fig. 6(c)] the oscillations go beyond the X arms, as for the focused X wave without OAM, because the spectrum becomes dominated at these large distances by the cutoff frequency [Fig. 6(f)].

An approximate expression for the radial distribution of frequencies at the focused X wave temporal center, $t' = 0$, can be obtained as for X waves. Equating the argument of $J_m(x)$, with $x = k_\perp(\omega)r$ and $k_\perp(\omega)$ given by (2), to the location of the first rise of $J_m(x)$, $x \simeq |m|$, we obtain a quadratic equation in

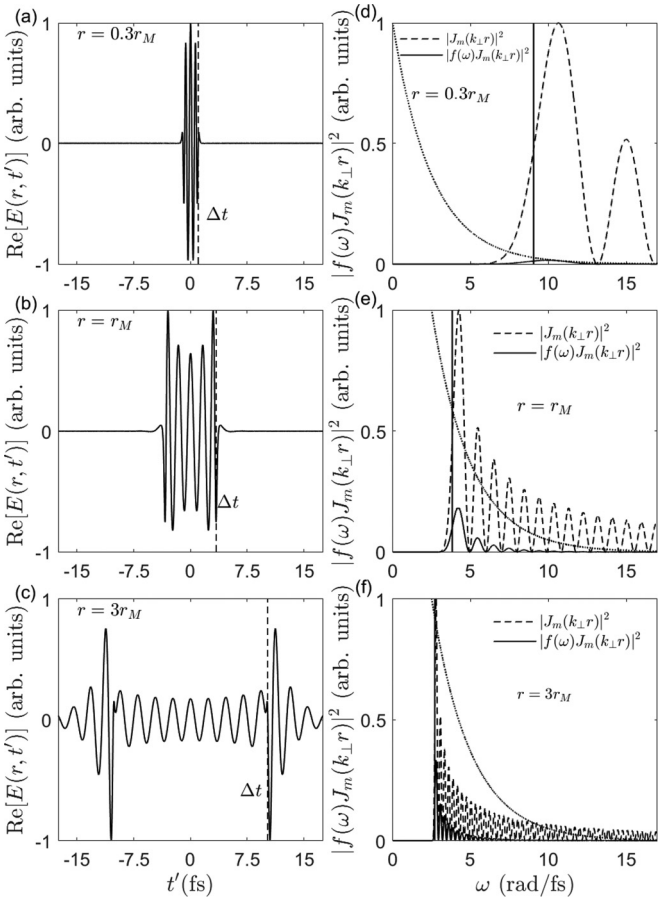

FIG. 6. [(a)–(c)] Real electric field of focused X waves with $v_g = 0.0004$ mm/fs, $\omega_z = 2.5$ rad/fs, $\epsilon = 0.2$ fs, and $|m| = 8$ at $r = 0.3r_M$, $r = r_M$, and $r = 3r_M$, where the radius of maximum fluence is given by (15). $\Delta t = (\sin\theta/c)r$ indicates the location of the X arms. (d–f) Respective power spectra (solid curves), the Bessel factor $J_m(k_\perp r)$ (dashed curves), and the broadband spectrum factor $f(\omega) = e^{-\epsilon\omega}$ (dotted curves). The vertical lines indicate the central frequency $\omega_c(r)$ given by (14), and coinciding with the rise of the Bessel functions in each case.

ω the positive solution of which is

$$\omega_c(r) \simeq \omega_z + \frac{c^2}{\sin^2\theta}\left(-\frac{a}{c} + \sqrt{\frac{a^2}{c^2} + \frac{\sin^2\theta}{c^2}\frac{m^2}{r^2}}\right), \qquad (14)$$

which is independent of ϵ, as for X waves, and approaches ω_z at large radius, as expected [Fig. 7(a)]. Expression (14) only fails in the close vicinity of the vortex, where the frequency becomes ϵ dependent and reaches approximately the same value $\omega_c(0) \simeq (|m| + 1)/\epsilon$ as for X waves.

We also observe that the central frequency $\omega_c(r_M)$ at the ring of maximum fluence is substantially independent of $|m|$ [Fig. 7(a)] and determined solely by the frequency where $|f(\omega)|^2 = e^{-2\epsilon\omega}$ has decayed approximately the same value $1/1.7 = 0.588$ as for X waves from its value at the cutoff frequency ω_z, i.e., $\omega_f' = \omega_z + \ln(1.7)/2\epsilon$. Equating ω_f' to $\omega_c(r)$ in (14), we obtain, after some algebra, the radius of maximum

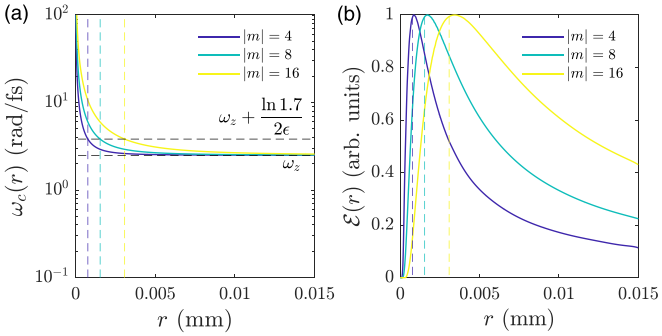

FIG. 7. (a) Central instantaneous frequency of the oscillations, $\omega_c(r)$, as a function of the radius r for the indicated values of $|m|$ of focused X waves with $v_g = 0.0004$ mm/fs, $\epsilon = 0.2$ fs, and $\omega_z = 2.5$ rad/fs as given by the approximate expression (14). In the immediate vicinity of the vortex singularity $\omega_c(r)$ does not approach infinity but to $\omega_c(0) \simeq (m+1)/\epsilon$. (b) Radial profiles of fluence of the same focused X waves, numerically evaluated from (12), and normalized to their peak values. In (a) and (b) the vertical lines are r_M given by (13), locating approximately the radii of maximum fluence. The horizontal lines in (a) help to visualize that the central instantaneous frequency $\omega_f' = \omega_z + \ln(1.7)/2\epsilon$ is the same at the respective radii of maximum fluence, i.e., independent of m, and that the frequency approaches ω_z at large radius. Violet (dark gray), green (gray), and yellow (light gray) curves are for $|m| = 4, 8, 16$, respectively.

fluence as

$$r_M \simeq \frac{|m|}{\sqrt{\omega_f^2 \frac{\sin^2\theta}{c^2} + 2\omega_f \frac{a}{c}}}. \tag{15}$$

Expression (15) provides a reasonably good approximation to the radius of maximum fluence [Fig. 7(b)]. This radius continues to be proportional to $|m|$, but is smaller than for X waves.

III. CONCLUSIONS

We have described the strongly coupled spatiotemporal structure of broadband superluminal localized waves with OAM. Temporal oscillations at all the frequencies in the broadband spectrum are displayed at different radii between the X arms, with a fixed number of oscillations dictated by OAM. A steep redshift with radial distance in conjunction with a pronounced blueshift of the whole X wave or focused X wave with the magnitude of the topological charge results in an invariant color at the ring of maximum energy density, the frequency of which is only determined by the spectrum of Bessel beams (which would directly be related to the spectrum of the laser source).

Of course, these X and focused X waves with OAM can only be created over a finite aperture, e.g., of radius R. For X waves, the cone angle θ, and hence the diffraction-free distance $z_{\text{free}} = R/\tan\theta$, are the same for all monochromatic Bessel beam constituents. X waves are then expected to diffract at this distance. For focused X waves, the maximum cone angle is just the cone angle θ of the X wave of the same group velocity, corresponding to a minimum diffraction-free distance equal to that of the X wave, where the focused X wave would start to diffract. Note that for X waves truncation at R involves truncation of the low frequencies located at radii larger than R. Finite-energy X waves with OAM would then acquire additional temporal oscillations in the form of sidelobes (similar to those of focused X waves because of truncation at ω_z), and would be, as focused X waves, only approximately minimal OAM carriers.

The scalar theory used in this paper is fully justified under paraxial conditions, e.g., the cone angles are not too steep. This is the actual situation in all recent experiments [6,7], particularly the very recent generation of localized waves (space-time wave packets) of picosecond duration carrying, for the first time, OAM [28]. Under nonparaxial conditions, the scalar theory is the basis for constructing electric and magnetic vector solutions to the Maxwell equations following, for example, the method of Hertz potentials [29].

The practical generation of these diffraction-free, dispersion-free, self-healing, and minimal OAM-carrier wave modes of femtosecond duration at visible frequencies would have an impact in obvious applications such as free-space, classical, and quantum communication systems [24–26] currently using Laguerre-Gauss modes as OAM carriers. In strong-field, nonperturbative light-matter interactions such as in the generation of high harmonics and attosecond pulses with OAM [30–32], replacing the standard Laguerre-Gauss modes with OAM-carrying X waves would enormously lengthen the depth of focus where light and matter can interact with a more uniform axial field.

We have deliberately left subluminal localized waves with OAM aside since they are expected to follow completely different rules as the transversal wave-number dispersion is not hyperbolic but elliptical. This analysis is deferred for further work.

ACKNOWLEDGMENTS

M.A.P. acknowledges support from Projects of the Spanish Ministerio de Ciencia, Innovación y Universidades Grants No. PGC2018-093854-B-I00 and No. FIS2017-87360-P.

[1] J. Lu and J. F. Greenleaf, Nondiffracting X waves-exact solutions to free-space scalar wave equation and their finite aperture realizations, IEEE Trans. Ultrason. Ferroelectr. Freq. Control **39**, 19 (1992).

[2] P. Saari and K. Reivelt, Evidence of X-Shaped Propagation-Invariant Localized Light Waves, Phys. Rev. Lett. **79**, 4135 (1997).

[3] P. Saari and K. Reivelt, Generation and classification of localized waves by Lorentz transformations in Fourier space, Phys. Rev. E **69**, 036612 (2004).

[4] *Localized Waves*, edited by H. E. Hernández-Figueroa, M. Zamboni-Rached, and E. Recami (Wiley, New York, 2008).

[5] *Non-Diffracting Waves*, edited by H. E. Hernández-Figueroa, E. Recami, and M. Zamboni-Rached (Wiley, New York, 2013).

[6] H. E. Kondakci and A. F. Abouraddy, Diffraction-free space-time light sheets, Nat. Photonics **11**, 733 (2017).

[7] B. Bhaduri, M. Yessenov, and A. F. Abouraddy, Meters-long propagation of diffraction-free space-time light-sheets, Opt. Express **26**, 20111 (2018).

[8] L. Allen, M. W. Beijersbergen, R. J. C. Spreeuw, and J. P. Woerdman, Orbital angular momentum of light and the transformation of Laguerre-Gaussian laser modes, Phys. Rev. A **45**, 8185 (1992).

[9] A. M. Yao and M. J. Padgett, Orbital angular momentum: origins, behavior and applications, Adv. Opt. Photon. **3**, 161 (2011).

[10] V. G. Shvedov, C. Hnatovsky, W. Krolikowski, and A. V. Rode, Efficient beam converter for the generation of high-power femtosecond vortices, Opt. Lett. **35**, 2660 (2010).

[11] K. Yamane, Y. Toda, and R. Morita, Ultrashort optical-vortex pulse generation in few-cycle regime, Opt. Express **20**, 18986 (2012).

[12] M. A. Porras, Upper Bound to the Orbital Angular Momentum Carried by an Ultrashort Pulse, Phys. Rev. Lett. **122**, 123904 (2019).

[13] M. A. Porras, Effects of orbital angular momentum on few-cycle and sub-cycle pulse shapes: coupling between the temporal and angular momentum degrees of freedom, Opt. Lett. **44**, 2538 (2019).

[14] M. A. Porras and R. García- Álvarez, General laws of the propagation of few-cycle optical pulses with orbital angular momentum in free space, Phys. Rev. A **102**, 033522 (2020).

[15] M. Ornigotti, C. Conti, and A. Szameit, Effect of Orbital Angular Momentum on Nondiffracting Ultrashort Optical Pulses, Phys. Rev. Lett. **115**, 100401 (2015).

[16] M. Ornigotti, C. Conti, and A. Szameit, Universal form of the carrier frequency of scalar and vector paraxial X waves with orbital angular momentum and arbitrary frequency spectrum, Phys. Rev. A **92**, 043801 (2015).

[17] M. A. Porras and C. Conti, Couplings between the temporal and orbital angular momentum degrees of freedom in ultrafast optical vortices, Phys. Rev. A **101**, 063803 (2020).

[18] S. Agasti and M. Ornigotti, Radial structure of OAM-carrying fundamental X-waves, Appl. Sci. **11**, 169 (2021).

[19] K. Pang, K. Zou, H. Song, Z. Zhao, A. Minoofar, R. Zhang, H. Song, H. Zhou, X. Su, C. Liu, N. Hu, M. Tur, and A. E. Willner, Simulation of near-diffraction- and near-dispersion-free OAM pulses with controllable group velocity by combining multiple frequencies, each carrying a Bessel mode, Opt. Lett. **46**, 4678 (2021).

[20] I. M. Besieris, M. Abdel-Rahman, A. M. Shaarawi and A. Chatzipetros, Two fundamental representations of localized pulse solutions to the scalar wave equation, Progress in Electromagnetic Research, PIER **19**, 1 (1998).

[21] D. Mugnai, A. Ranfagni, and R. Ruggeri, Observation of Superluminal Behaviors in Wave Propagation, Phys. Rev. Lett. **84**, 4830 (2000).

[22] H. Sõnajalg, M. Rätsep, and P. Saari, Demonstration of the Bessel-X pulse propagating with strong lateral and longitudinal localization in a dispersive medium, Opt. Lett. **22**, 310 (1997).

[23] S. Li and J. Wang, Adaptive free-space optical communications through turbulence using self-healing Bessel beams, Sci. Rep. **7**, 43233 (2017).

[24] H. Huang *et al.*, 100 Tbit/s free-space data link enabled by three-dimensional multiplexing of orbital angular momentum, polarization, and wavelength, Opt. Lett **39**, 197 (2014).

[25] C. Paterson, Atmospheric Turbulence and Orbital Angular Momentum of Single Photons for Optical Communication, Phys. Rev. Lett **94**, 153901 (2005).

[26] Y. Zhang, I. B. Djordjevic, and X. Gao, On the quantum-channel capacity for orbital angular momentum-based free-space optical communications, Opt. Lett. **37**, 3267 (2012).

[27] I. M. Besieris and A. M. Shaarawi, Spatiotemporally localized null electromagnetic waves, in *Non-Diffracting Waves*, edited by H. Hernandez-Figueroa, M. Zamboni-Rached and E. Recami (Wiley, New York, 2013), pp. 161–188.

[28] M. Yessenov, J. Free, Z. Chen, E. G. Johnson, M. P. J. Lavery, M. A. Alonso, and A. F. Abouraddy, Space-time wave packets localized in all dimensions, arXiv:2111.03095 v1 (2021).

[29] J. A. Stratton, *Electromagnetic Theory* (Dover, New York, 2010).

[30] C. Hernández-García, A. Picón, J. San Román, and L. Plaja, Attosecond Extreme Ultraviolet Vortices from High-Order Harmonic Generation, Phys. Rev. Lett. **111**, 083602 (2013).

[31] G. Gariepy, J. Leach, K. T. Kim, T. J. Hammond, E. Frumker, R. W. Boyd, and P. B. Corkum, Creating High-Harmonic Beams with Controlled Orbital Angular Momentum, Phys. Rev. Lett. **113**, 153901 (2014).

[32] L. Rego, J. S. Román, A. Picón, L. Plaja, and C. Hernández-García, Nonperturbative Twist in the Generation of Extreme-Ultraviolet Vortex Beams, Phys. Rev. Lett. **117**, 163202 (2016).